ACCELERATED HIGH-RESOLUTION RADIATIVE TRANSFER SIMULATION FOR CO_2 CONCENTRATION ESTIMATION FROM NANOCARB MEASUREMENTS

Jordan L. Tedongmo[1,2], **Yann Ferrec, Laurence Croizé**
[1]DOTA
ONERA – The French Aerospace Lab
Chemin de la Hunière, 80100, 91123 Palaiseau, France
{jordan.lontsi_tedongmo,yann.ferrec,laurence.croize}@onera.fr

Pablo Musé, Gabriele Facciolo
[2]Centre Borelli, CNRS, ENS Paris-Saclay
Université Paris-Saclay
91190 Gif-sur-Yvette, France
{pmuse,gabriele.facciolo}@ens-paris-saclay.fr

Andrés Almansa
[3]MAP5 UMR 8145, CNRS
Université Paris Cité
F-75006 Paris, France
andres.almansa@parisdescartes.fr

ABSTRACT

Studying climate change requires reducing uncertainties in CO_2 and CH_4 emission estimates to better distinguish anthropogenic from natural sources, which motivates spaceborne measurements with improved revisit frequency and spatial coverage. In this context, the Horizon Europe SCARBOn project assesses a low-cost satellite constellation featuring the NanoCarb imaging interferometer as its core sensor for monitoring CO_2 and CH_4 emissions in the atmosphere. However, estimating CO_2 and CH_4 concentrations from NanoCarb measurements poses significant challenges: full-physics retrieval algorithms commonly used rely on repeated high-resolution radiative transfer (RT) simulations, which are computationally expensive when using line-by-line RT models. As an alternative, we propose in this study a feedforward multilayer perceptron (MLP) surrogate designed to accurately and efficiently predict top-of-atmosphere radiances in the CO_2 weak band, using a combined mean absolute error (MAE) loss on radiances and RT Jacobians to preserve both spectral accuracy and sensitivity to geophysical parameters. Coupling the MLP-based RT surrogate with the NanoCarb instrumental response yields an efficient and precise forward model for NanoCarb measurements, which shows promising results for CO_2 concentration retrievals.

1 INTRODUCTION

Carbon dioxide (CO_2) and methane (CH_4) are major anthropogenic greenhouse gases (GHGs) whose emissions require accurate spatio-temporal monitoring, thereby supporting the mitigation efforts essential to achieving the Paris Agreement's goal (Naser & Pearce, 2022). In practice, while most current and planned satellite missions dedicated to GHGs monitoring achieve high sensitivity to GHG emissions, their spatial resolution and revisit frequency are still insufficient to detect and quantify anthropogenic emissions with required precision (Gousset et al., 2019).
Advancing these goals is one key motivation for the the Horizon Europe SCARBOn project, which assesses a low-cost satellite constellation featuring the miniature GHG sensor NanoCarb as its core

sensor for monitoring CO_2 and CH_4 emissions in the atmosphere (Gousset et al., 2019). Estimating GHGs concentrations from NanoCarb measurements then relies on the so-called full-physics retrieval (or inverse) algorithm, in which high-resolution radiative transfer (RT) calculations must be performed over the sensor response domain for each instrument channel to simulate the measurement according to the sensor's response function. However, commonly used line-by-line radiative transfer models (Clough & Iacono, 1995) are highly computationally intensive, posing significant challenges in operational contexts, especially for the NanoCarb concept, where the satellite constellation will generate vastly more data to process.

To overcome the computational limits of physics-based radiative transfer codes in retrieval algorithms, several studies have explored deep neural networks to emulate sensor measurements directly (Gao et al., 2021; Nanda et al., 2019; Stegmann et al., 2022; Liu & Liang, 2023); however, few address high spectral resolution RT in key GHG spectral bands (Le et al., 2020), and these methods have not yet been evaluated for GHG concentration retrievals. Other authors have used neural networks to solve the inverse problem directly (David et al., 2021; Reuter et al., 2025), but this approach lacks flexibility across varying instruments and observation conditions. Therefore, efficient atmospheric radiative transfer models capable of high-resolution calculations and adaptable to diverse instruments remain critically needed.

This paper presents a fast and accurate neural-network forward model for high-resolution CO_2 radiances simulations at the top of the atmosphere, describing its training and architecture. The proposed model is then applied in an inverse retrieval framework for CO_2 total column and surface albedo estimation from synthetic NanoCarb data, highlighting its potential as a computationally efficient alternative to conventional radiative transfer models.

2 Forward and inverse models for CO2 estimation from NanoCarb measurements

The NanoCarb sensor (Gousset et al., 2017) is a static Fourier-transform imaging spectrometer using a low-finesse Fabry–Perot (FP) array for partial interferometric sampling, enabling wide-swath, high-resolution snapshot measurements. The analytical model (Gousset et al., 2019) expresses the focal-plane intensity from the FP transmission function, defined for monochromatic radiation as:

$$T_{FP} \approx \frac{1}{1 + M \sin^2\left(\frac{\varphi}{2}\right)}, \tag{1}$$

where M is the finesse and $\varphi = 2\pi\sigma\delta$ the phase shift for wavenumber σ and optical path difference δ. By adjusting their mechanical thicknesses ε_i, the FP interferometers are tuned to match the absorption lines of key greenhouse gases (CO_2, CH_4, O_2), while the OPD variation $\delta(\sigma, i, \theta, T) = 2n(\sigma, T)\varepsilon_i \cos\theta_r$ accounts for dependencies on refractive index, temperature, and incidence angle. This allows each NanoCarb pixel to record a partial interferogram I-with 81 FP thicknesses (channels) for the CO_2 airborne prototype used in this study—highly sensitive to the targeted GHG concentration, but also to surface albedo and possibly other atmospheric parameters (such as water vapor, aerosols, etc.). Integration of the FP-transmitted terrestrial radiance over the considered spectral band $\Delta\sigma$ allows to derive the interferogram as a function of the OPD as :

$$I_\delta = \eta \int_{\Delta\sigma} \left(\frac{1}{hc\sigma}\right) T_\sigma T_{FP} L_\sigma d\sigma, \text{[e/frame/pixel]}, \tag{2}$$

where L_σ is the spectral radiance, T_σ the instrument transmission, and $\eta = \Omega S t_{\text{exp}} T_{\text{opt}}$ the optical–radiometric efficiency. Simulating NanoCarb measurements therefore requires computing high-resolution spectral radiances using a line-by-line radiative transfer model.

The retrieval process then estimates the gas concentration and other parameters by minimizing the difference between measured and simulated interferograms, as described in the well known optimal estimation method (Rodgers, 2000) implemented in this study.

3 Neural Network forward model

3.1 Training Data

To train our NN RT model, we generated synthetic training data by sampling key atmospheric parameters contributing to the radiance formation in the CO_2 weak band at 3 km altitude (airborne

sensor height), neglecting aerosols. Simulations were performed with the 4AOP radiative transfer code Scott & Chedin (1981); Scott (1974) using the HITRAN spectroscopic database Rothman et al. (2009). Inputs include CO_2 total-column, surface properties (albedo, altitude, pressure), solar–sensor geometry (solar and viewing zenith angles), and vertical profiles of temperature and water vapour from the TIGR database Rothman et al. (2009). RT simulations use full profiles, while NN training employs a reduced representation: a total-column scaling for CO_2 concentration, and temperature/water vapour projected onto a low-dimensional PCA basis. Using the distributions in Table 1 (see appendix), we generated 70,000 scenarios and computed their radiances (6175–6250 cm^{-1} at 0.01 cm^{-1} resolution 7,499 channels) and Jacobians w.r.t. all inputs parameters.
To evaluate the NN forward model, an independent test set of $\approx 6,000$ cases was generated by randomly selecting 200 temperature and H_2O profiles from TIGR (excluded from training) and sampling the remaining parameters as in Table 1, except for albedo, which was varied between 0.05 and 0.7. For this set, both high-resolution radiances and corresponding NanoCarb interferograms were simulated for an end-to-end assessment of NN performance.
By sampling key atmospheric and surface parameters over broad intervals, together with using temperature and water vapour profiles from the TIGR database (measured across different regions and seasons), this dataset covers a wide range of realistic atmospheric and surface conditions, providing good geospatial representativity.

3.2 Neural Network architecture and Training

Our NN radiative transfer surrogate is a feedforward multilayer perceptron (MLP). All inputs are concatenated into a single feature vector x ($n_f = \dim(x) = 20$; Table 1), and the network outputs the full high-resolution radiance spectrum with $n_\sigma = 7{,}499$ channels, one per output neuron. Training optimizes the MLP parameters θ (weights and biases) by minimizing a joint loss on radiances and Jacobians. Inputs and outputs are normalized for stability: c_j denotes the raw input for scenario j, with x_j its normalized form; $L_\sigma(c_j)$ is the RT-computed radiance spectrum, and $y_F(x_j)$ its normalized counterpart. The NN then predicts a normalized radiance spectrum $y_\theta(x_j) \in \mathbb{R}^{n_\sigma}$, with the loss defined as:

$$\mathcal{L}(\theta) = \frac{1}{N\, n_\sigma} \sum_{j=1}^{N} \sum_{t=1}^{n_\sigma} \left| y_\theta^{(t)}(x^{(j)}) - y_F^{(t)}(x^{(j)}) \right| + \mathcal{L}_{\mathrm{Jac}}(\theta), \tag{3}$$

where N is the number of training samples and $n_\sigma = 7{,}499$ the number of spectral channels. The use of a Jacobian loss term, already introduced by Liu & Liang (2023), enforces physical consistent sensitivities to input parameters and also regularizes training:

$$\mathcal{L}_{\mathrm{Jac}}(\theta) = \sum_{i=1}^{n_f} \alpha_i \, \frac{1}{N\, n_\sigma} \sum_{j=1}^{N} \sum_{t=1}^{n_\sigma} \left| J_\theta^{(t,i)}(x^{(j)}) - J_F^{(t,i)}(x^{(j)}) \right|, \tag{4}$$

where $J_X^{(t,i)}(x^{(j)}) = \frac{\partial y_X^{(t)}(x^{(j)})}{\partial x_i^{(j)}}$ are the Jacobians, computed using finite differences for J_F and forward-mode automatic differentiation Baydin et al. (2018); PyTorch Team (2023) for J_θ, and the weights α_i balance the contribution of each input parameter x_i, defined from the mean radiance sensitivities to input parameters, as $\alpha_i \propto y_{\mathrm{mean}}/|J_{\mathrm{mean}}^{(i)}|$ (with y_{mean} the mean radiance and $J_{\mathrm{mean}}^{(i)}$ the mean Jacobian magnitude w.r.t. x_i).
For the network architecture, multiple configurations were explored, leading to the selection of an MLP with three hidden layers of 100, 500, and 3,500 neurons and ELU activations, offering the best trade-off between accuracy and computational efficiency.

4 Results

We first evaluate the performance of the trained NN RT model together with the NN-based NanoCarb forward model, which combines the NanoCarb instrumental model and the NN RT model as expressed in equation 2. The assessment is carried out using the $\approx 6,000$ specially simulated test examples. Results summarized in Figure 1 indicate that the models reproduce the radiances and partial interferograms with very high accuracy, achieving an overall mean absolute relative error below 0.04% across all channels. Errors approach 0.1% only for the albedo 0.05 cases, while for an albedo of 0.2, similar accuracy is maintained across all channels (FP thicknesses) for interferogram, with

just a few wavelengths reaching 0.1% for radiance.
The NN-based NanoCarb forward model is integrated into the retrieval algorithm (Sect. 2) to estimate the CO_2 total column (X_{CO_2}) and surface albedo, with remaining parameters treated as known.

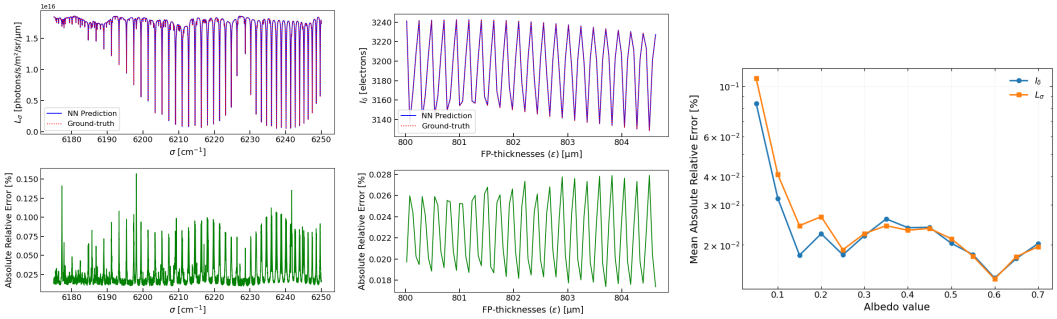

(a1) (a2) (b)

Figure 1: Panels (a1) and (a2) compare the averaged neural network predictions with the averaged radiative transfer (RT) simulations (ground truth) for an albedo of 0.2, with lower plots showing the corresponding averaged absolute relative errors across channels for Radiance and Interferograms. Panel (b) displays the mean absolute relative error for Radiance (orange) and Interferograms (blue) predictions over all test cases as a function of albedo.

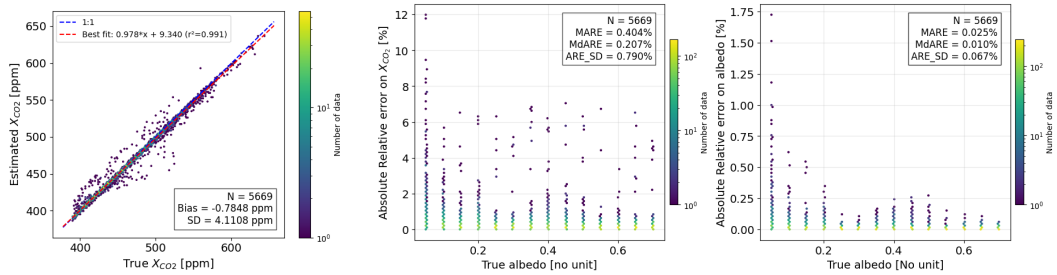

(a) (b)

Figure 2: Density histograms summarizing the CO_2 total column retrievals (a) and associated errors (b) estimated from NanoCarb interferometric measurements simulated with the 4AOP RT model and inverted using our neural network–based forward model.

The algorithm, applied to $\approx$ 6,000 noise-free simulated NanoCarb measurements, isolates the impact of the NN approximation on retrieval accuracy. As shown in Fig. 2, retrieved X_{CO_2} and albedo exhibit very low uncertainties—below 0.5% and 0.025%, respectively—with largest deviations observed for low-albedo cases. The approach achieves significant computational gains, running up to 150× faster on CPU and over 400× faster on GPU compared to the reference implementation.

5 Conclusions and Future Work

The proposed NN-based radiative transfer and NanoCarb forward models accurately reproduce radiances and interferograms, with mean relative errors below 0.04% and up to 0.1% only at low albedo. When applied in the retrieval algorithm, they yield CO_2 and albedo uncertainties below 0.5% and 0.025%, respectively, while accelerating computations by over two orders of magnitude—making the approach suitable for operational use as an initial guess in NanoCarb retrieval processing. The proposed methodology can also be extended to other SWIR GHG bands and sensors, with future work addressing aerosol effects and integration into more advanced inversion schemes.

REFERENCES

Atilim Gunes Baydin, Barak A Pearlmutter, Alexey Andreyevich Radul, and Jeffrey Mark Siskind. Automatic differentiation in machine learning: a survey. *Journal of machine learning research*, 18(153):1–43, 2018.

Shepard A Clough and Michael J Iacono. Line-by-line calculation of atmospheric fluxes and cooling rates: 2. application to carbon dioxide, ozone, methane, nitrous oxide and the halocarbons. *Journal of Geophysical Research: Atmospheres*, 100(D8):16519–16535, 1995.

Leslie David, François-Marie Bréon, and Frédéric Chevallier. XCO_2 estimates from the OCO-2 measurements using a neural network approach. *Atmospheric Measurement Techniques*, 14(1): 117–132, 2021. doi: 10.5194/amt-14-117-2021.

Meng Gao, Bryan A Franz, Kirk Knobelspiesse, Peng-Wang Zhai, Vanderlei Martins, Sharon Burton, Brian Cairns, Richard Ferrare, Joel Gales, Otto Hasekamp, et al. Efficient multi-angle polarimetric inversion of aerosols and ocean color powered by a deep neural network forward model. *Atmospheric Measurement Techniques Discussions*, 2021:1–41, 2021.

S Gousset, E Le Coarer, N Guérineau, L Croizé, T Laveille, and Y Ferrec. Nanocarb-21: a miniature fourier-transform spectro-imaging concept for a daily monitoring of greenhouse gas concentration on the earth surface. In *International Conference on Space Optics—ICSO 2016*, volume 10562, pp. 1411–1419. SPIE, 2017.

Silvère Gousset, Laurence Croizé, Etienne Le Coarer, Yann Ferrec, Juana Rodrigo-Rodrigo, Laure Brooker, and SCARBO consortium http://scarbo-h2020. eu/. Nanocarb hyperspectral sensor: on performance optimization and analysis for greenhouse gas monitoring from a constellation of small satellites. *CEAS Space Journal*, 11(4):507–524, 2019.

Tianhao Le, Chao Liu, Bo Yao, Vijay Natraj, and Yuk L. Yung. Application of machine learning to hyperspectral radiative transfer simulations. *Journal of Quantitative Spectroscopy and Radiative Transfer*, 246:106928, 2020. doi: 10.1016/j.jqsrt.2020.106928.

Quanhua Liu and XingMing Liang. Physics constraint deep learning based radiative transfer model. *Optics Express*, 31(17):28596–28610, 2023.

Swadhin Nanda, Martin de Graaf, Maarten Sneep, Johan F. de Haan, Piet Stammes, Alma F. J. Sanders, Olaf N. E. Tuinder, J. Pepijn Veefkind, and Pieternel F. Levelt. A neural network radiative transfer model approach applied to the Tropospheric Monitoring Instrument aerosol height algorithm. *Atmospheric Measurement Techniques*, 12(12):6619–6634, 2019. doi: 10.5194/amt-12-6619-2019.

Mostafa Mahmud Naser and Prafula Pearce. Evolution of the international climate change policy and processes: Unfccc to paris agreement. In *Oxford Research Encyclopedia of Environmental Science*. 2022.

PyTorch Team. Forward-mode automatic differentiation (beta), Updated: Apr 18 2023. URL `https://pytorch.org/docs/stable/tutorials/intermediate/forward_ad_usage.html`. Accessed: 2025-09-05.

Maximilian Reuter, Michael Buchwitz, Oliver Schneising, Stefan Noel, Heinrich Bovensmann, and John P. Burrows. Retrieving the atmospheric concentrations of carbon dioxide and methane from the European Copernicus CO2M satellite mission using artificial neural networks. *Atmospheric Measurement Techniques*, 18(1):241–264, 2025. doi: 10.5194/amt-18-241-2025.

Clive D. Rodgers. *Inverse Methods for Atmospheric Sounding: Theory and Practice*, volume 2. World Scientific, 2000. doi: 10.1142/3171.

Laurence S Rothman, Iouli E Gordon, Alain Barbe, D Chris Benner, Peter F Bernath, Manfred Birk, Vincent Boudon, Linda R Brown, Alain Campargue, J-P Champion, et al. The hitran 2008 molecular spectroscopic database. *Journal of Quantitative Spectroscopy and Radiative Transfer*, 110(9-10):533–572, 2009.

NA Scott. A direct method of computation of the transmission function of an inhomogeneous gaseous medium—i: Description of the method. *Journal of Quantitative Spectroscopy and Radiative Transfer*, 14(8):691–704, 1974.

NA Scott and Alain Chedin. A fast line-by-line method for atmospheric absorption computations: The automatized atmospheric absorption atlas. *Journal of Applied Meteorology (1962-1982)*, pp. 802–812, 1981.

Patrick G Stegmann, Benjamin Johnson, Isaac Moradi, Bryan Karpowicz, and Will McCarty. A deep learning approach to fast radiative transfer. *Journal of Quantitative Spectroscopy and Radiative Transfer*, 280:108088, 2022.

A APPENDIX

Table 1: Parameters used to generate the synthetic training dataset for the neural network radiative transfer model (aerosols not included).

Parameter	Unit	Min	Max	Sampling strategy	Dim.
CO_2total column (X_{CO_2})	ppm	390	650	$\mathcal{N}(\mu = 423,\ \sigma = 0.15\mu)$	1
Surface albedo (A)	–	10^{-3}	1	$\log_{10}(A) \sim \mathcal{N}(\mu = \log_{10}(0.3),\ \sigma = 0.7\lvert\mu\rvert)$	1
Viewing zenith angle (VZA)	deg	0	15	$\mathcal{U}(0, 20)$, step 1°	1
Solar zenith angle (SZA)	deg	0	80	$\mathcal{U}(0, 80)$, step 2°	1
Surface altitude (H_{surf})	m	0	1200	$\mathcal{N}(\mu = 300,\ \sigma = 300)$	1
Surface pressure (P_{surf})	hPa	940	1060	$\mathcal{U}(940, 1060)$, step 1 hPa	1
Temperature profile ($T(z)$)	K	–	–	2311 TIGR profiles + PCA	8
Water vapour profile ($X_{H_2O}(z)$)	g/g	–	–	2311 TIGR profiles + PCA	6